IJCSI International Journal of Computer Science Issues, Volume 13, Issue 6, November 2016
ISSN (Print): 1694-0814 | ISSN (Online): 1694-0784
www.IJCSI.org https://doi.org/10.20943/01201606.8897

Modeling and simulation of multi-disk auto-balancing rotor

YANG Yi-jiao[1, 2, 3, 4], TAN Qing[1, 3], YI Nian-en[1, 3,*], YANG Jun-zhe[2]

[1.]State Key Laboratory of High Performance Complex Manufacturing, Central South University, Changsha, Hunan 410083, China

[2.]School of Automotive and Mechanical Engineering, Changsha University of Science and Technology, Changsha, Hunan, 410114, China

[3.]School of Mechanical and Electrical Engineering, Central South University, Changsha, Hunan 410083, China

[4.]Key Laboratory of Safety Design and Reliability Technology for Engineering Vehicle, Hunan Province, Changsha, Hunan, 410114, China

Abstract

Mathematical model of multi-disk auto-balancing rotor has been established by Lagrange equation. By simulation, it found that the ball was moved automatically to the opposite side of eccentric mass with balancing the eccentric mass automatically and reducing vibration when the tri-disk auto-balancing rotor reached above third order critical rotation speed; The ball was moved automatically to the same side of the eccentric mass, enlarging eccentric mass and increasing the vibration when below first order critical rotation speed; Regarding distributions on the same side with eccentric mass, vibration was reduced when they are between first order and second order critical rotation speeds; Regarding distributions on the same side with eccentric mass and on the asymmetric opposite side, vibration was reduced, when they are between second order and third order critical rotation speeds; Vibration was increased in other situations.

Keywords: *rotor dynamics; auto-balancing; modeling; simulation; eccentric mass*

1. Introduction

Automatic balancing is an ideal way to solve unbalanced rotor vibration. Single-disk auto-balancing rotor has been widely studied[1-12], yet whether its performance could be applied in the multi-disk rotor remains a topic to be researched. In this paper, it attempted to establish an auto-balancing mathematical model of multi-disk rotor. Tri-disk rotor was taken as an example to carry out simulation analysis.

2. Numerical modeling

Tri-disk auto-balancing rotor is shown in Fig. 1.

O_{01} (O_{02},O_{03}), O_1(O_2,O_3), G_1(G_2,G_3) is the rotational center, geometric center, mass center of disk 1(2, 3) respectively. Assuming that a driving torque of a motor is large enough, drag torque changed and rotation speed remained constant while load changed, excluding shaft torsional vibration; With linear damping, the ball was rolling purely; Stiffness of bearing seat was large enough to ignore deformation of the bearing; The disk center was on the center line of the revolving shaft. Inside the disk, raceway and lubricants are applied. The ball moves along its raceway and the number of them should be no less than 2. Furthermore, its spindle is vertical and the disk revolves on a horizontal plane.

By adopting Lagrange equation, a mathematical model of tri-disk auto-balancing rotor can be established:

$$
\begin{cases}
M_1\ddot{X}_1 + c_1\dot{X}_1 + c_2\left(\dot{X}_1 - \dot{X}_2\right) + k_1X_1 + k_2\left(X_1 - X_2\right) = m_{p1}e_1\omega^2\cos\omega t + \sum_{j=1}^{n_i} m_{q1}R_1\left(\dot{\phi}_{1j}\right)^2\cos\phi_{1j}\right) \\
M_1\ddot{Y}_1 + c_1\dot{Y}_1 + c_2\left(\dot{Y}_1 - \dot{Y}_2\right) + k_1Y_1 + k_2\left(Y_1 - Y_2\right) = m_{p1}e_1\omega^2\sin\omega t + \sum_{j=1}^{n_i} m_{q1}R_1\dot{\phi}_{1j}^{\ 2}\sin\phi_{1j} \\
M_2\ddot{X}_2 + c_2\left(\dot{X}_2 - \dot{X}_1\right) + c_3\left(\dot{X}_2 - \dot{X}_3\right) + k_2\left(X_2 - X_1\right) + k_3\left(X_2 - X_3\right) = m_{p2}e_2\omega^2\cos\omega t + \sum_{j=1}^{n_i} m_{q2}R_2\dot{\phi}_{2j}^{\ 2}\cos\phi_{2j} \\
M_2\ddot{Y}_2 + c_2\left(\dot{Y}_2 - \dot{Y}_1\right) + c_3\left(\dot{Y}_2 - \dot{Y}_3\right) + k_2\left(Y_2 - Y_1\right) + k_3\left(Y_2 - Y_3\right) = m_{p2}e_2\omega^2\sin\omega t + \sum_{j=1}^{n_i} m_{q2}R_2\dot{\phi}_{2j}^{\ 2}\sin\phi_{2j} \\
M_3\ddot{X}_3 + c_3\left(\dot{X}_3 - \dot{X}_2\right) + c_4\dot{X}_3 + k_3\left(X_3 - X_2\right) + k_4X_3 = m_{p3}e_3\omega^2\cos\omega t + \sum_{j=1}^{n_i} m_{q3}R_3\dot{\phi}_{3j}^{\ 2}\cos\phi_{3j} \\
M_3\ddot{Y}_3 + c_3\left(\dot{Y}_3 - \dot{Y}_2\right) + c_4\dot{Y}_3 + k_3\left(Y_3 - Y_2\right) + k_4Y_3 = m_{p3}e_3\omega^2\sin\omega t + \sum_{j=1}^{n_i} m_{q3}R_3\dot{\phi}_{3j}^{\ 2}\sin\phi_{3j} \\
\left(m_{qi} + \frac{I_i}{r_i^2}\right)R_i\ddot{\phi}_{ij} + \beta_{i1}R_i\left(\dot{\phi}_{ij} - \omega\right) + \frac{\beta_{i0}}{r_i}m_{qi}R_i\dot{\phi}_{ij}^{\ 2}\,\mathrm{sgn}(\dot{\phi}_{ij} - \omega) = m_{qi}\left(\ddot{X}_i\sin\phi_{ij} - \ddot{Y}_i\cos\phi_{ij}\right) \\
\left(i = 1,2,3;\ j = 1,2,\cdots,n_i\right)
\end{cases}
$$

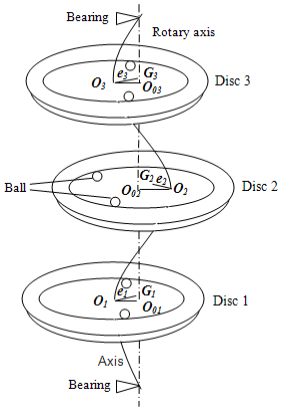

Fig. 1 Tri-disk auto-balancing rotor diagram

3. Simulation analysis

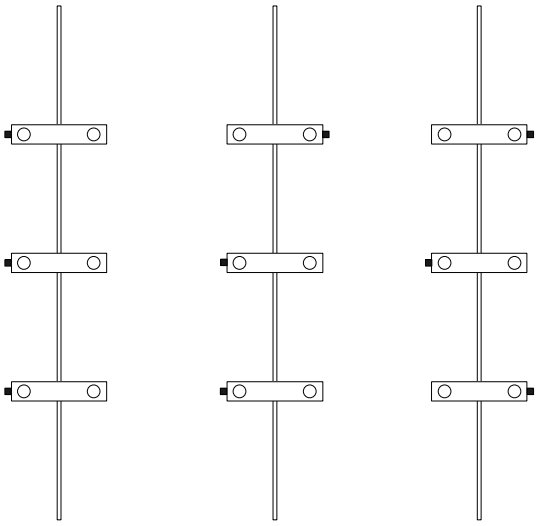

(a)Same side (b)Asymmetric opposite side (c)Symmetric opposite side

Fig. 2 Plane distribution of eccentric mass.

The plane distributions of the eccentric mass are shown in fig. 2.

Simulation parameters are shown in Table 1.

Table 1 Simulation parameters

parameters	*units*	*value*
r_i	m	0.050
e	m	0.050
m_{qi}	Kg	0.020
m_{pi}	Kg	0.020
M_i	Kg	2.459
k_1		5032.32
k_2		20129.28
k_3		20129.28
k_4		5032.32
c_i		5.6
β_{i0}		0.0000415
β_{i1}		0.03678
ω_{n1}	Hz	12.527
ω_{n2}	Hz	23.752
ω_{n3}	Hz	33.096
ϕ_{110}	radian	0.5
ϕ_{120}	radian	1.0
ϕ_{210}	radian	1.5
ϕ_{220}	radian	2.0
ϕ_{310}	radian	2.5
ϕ_{320}	radian	3.0

Figure presentation can be defined as:

Steady-state location diagram of the rotor: solid circle represents the location of eccentric mass, hollow circle, the location of the ball, solid points and cross-star, 100000 times of steady-state amplitude position of

auto-balancing rotor and common rotor.

Phase variation process diagram of the ball: vertical coordinate represents the phase of the ball.

Resultant amplitude diagram of the rotor: it indicates variation process of resultant amplitude. Auto-balancing rotor is on the upper side, while common rotor on the lower side.

The orbit diagram of the shaft center: auto-balancing rotor is on the left side, while common rotor is the right side.

According to the vibrating mode theory and the inherent frequency of rotor system the simulation results of supercritical speed of rotation are shown in fig. 3, 4, 5, while the steady-state resultant amplitude of supercritical speed of rotation is shown in table 2 and the steady-state phase of ball at supercritical speed of rotation is shown in table 3. It shows that the ball is moved automatically to the opposite side of the eccentric mass and evenly distributed with the eccentric mass with steady-state resultant amplitude decreasing significantly; Moving from the initial phase, each ball reaches its stable phase upon 25 s; Resultant amplitude of auto-balancing rotor has a step-by-step dynamic process of decreasing; Shaft center orbit of auto-balancing rotor is solid circle in convergence, while that of common rotor is hollow circle in divergence.

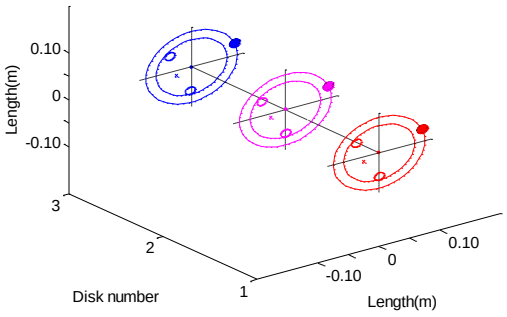

(a) Steady-state location diagram of ball, eccentric mass and centroid

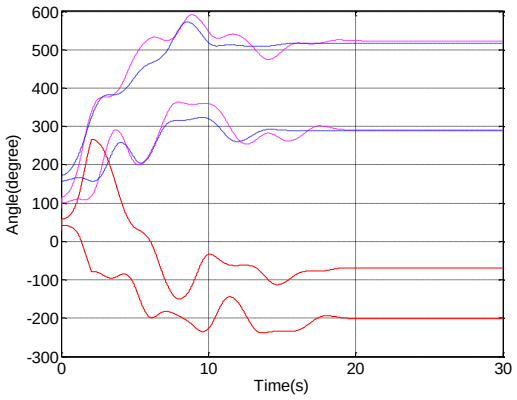

(b) Phase variation process diagram of the ball

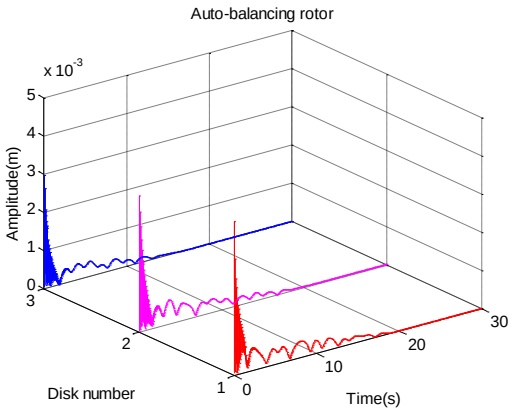

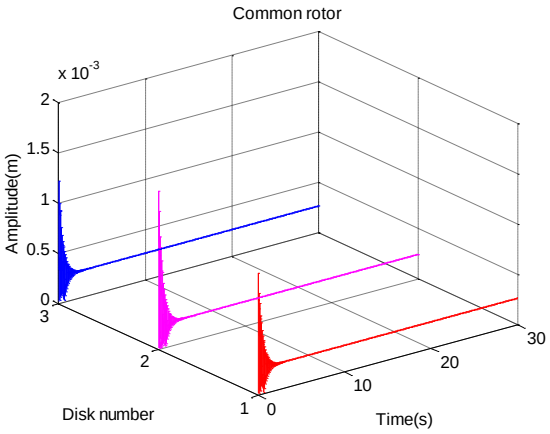

(c) Resultant amplitude diagram of rotor

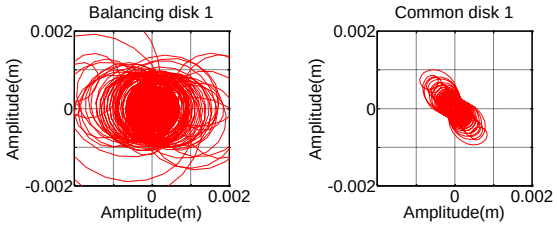

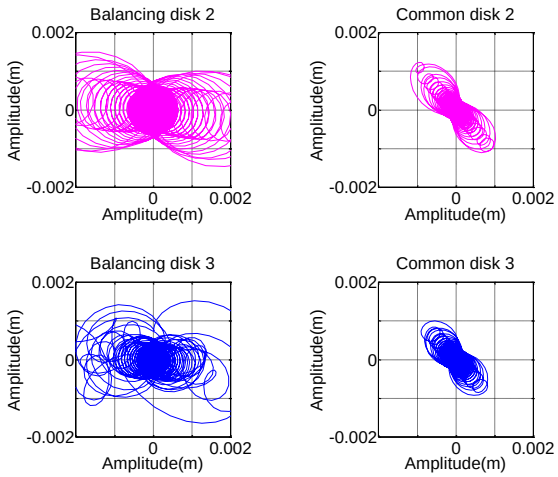

(d) Orbit diagram of the shaft center

Fig. 3 Simulation results of same side distribution whenω =20Hz

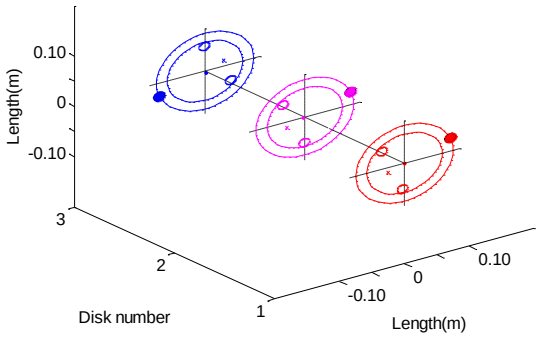

(a) Steady-state location diagram of ball, eccentric mass and centroid

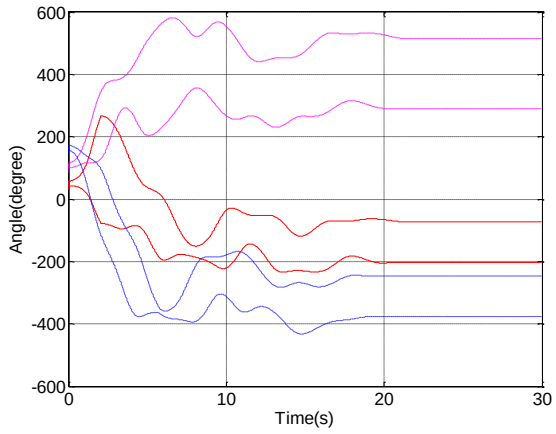

(b) Phase variation process diagram of the ball

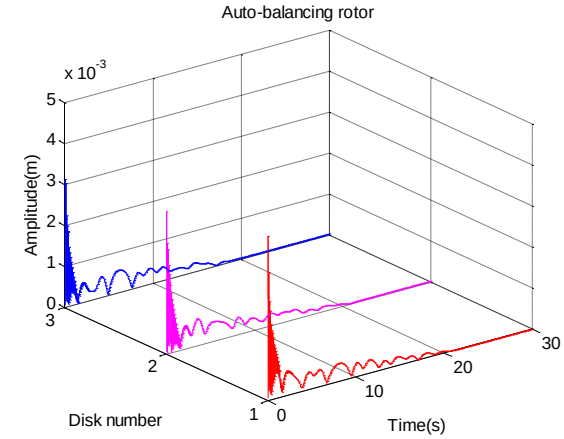

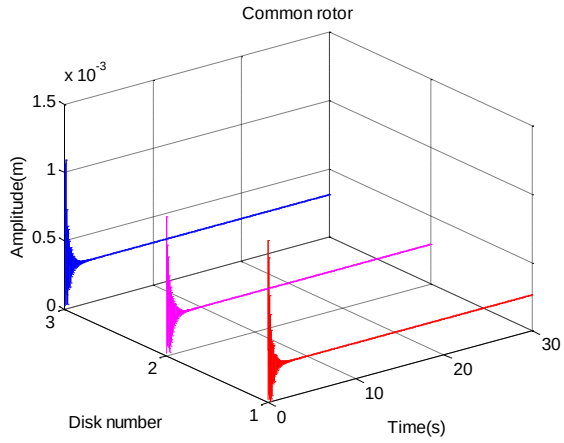

(c) Resultant amplitude diagram of rotor

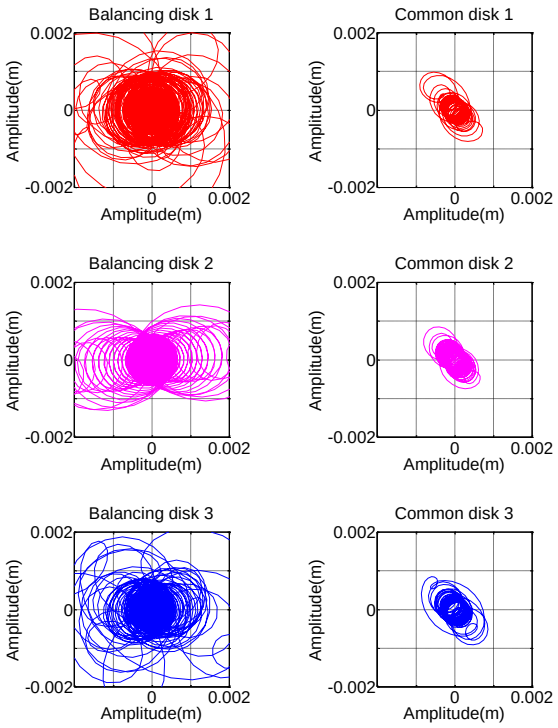

(d) Orbit diagram of the shaft center

Fig. 4 Simulation results of asymmetric opposite side distribution when

ω =30Hz

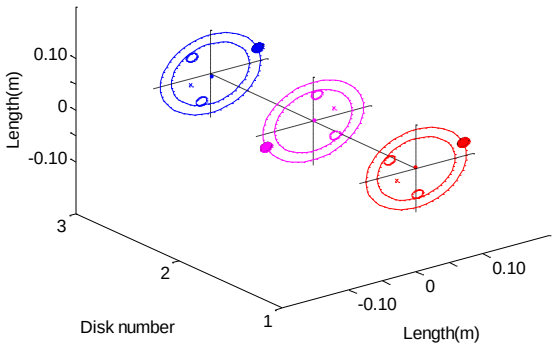

(a) Steady-state location diagram of ball, eccentric mass and centroid

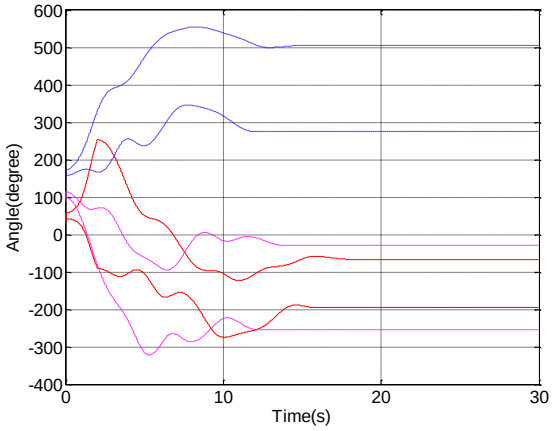

(b) Phase variation process diagram of the ball

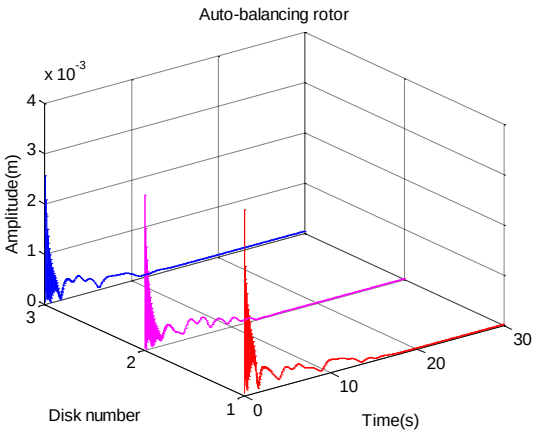

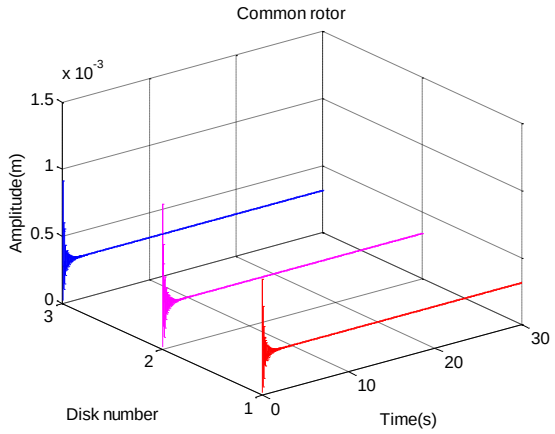

(c) Resultant amplitude diagram of rotor

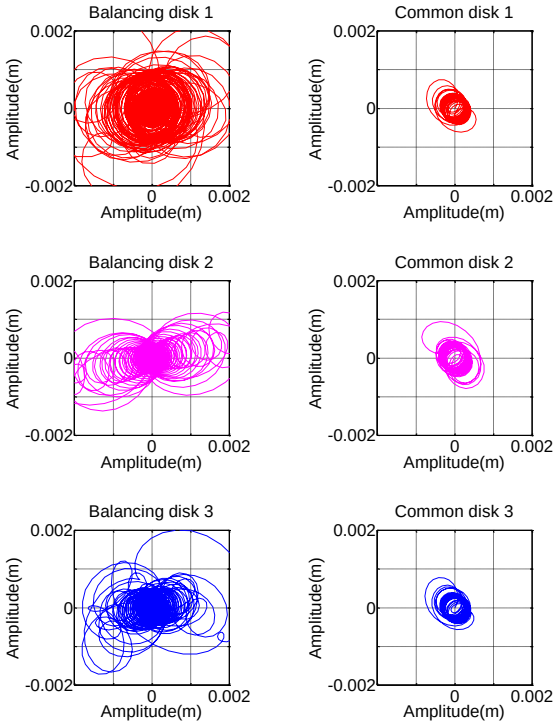

(d) Orbit diagram of the shaft center

Fig. 5 Simulation results of the symmetric opposite side distribution whenω =45

Table 2 Steady-state resultant amplitude at supercritical speed (unit: 10^{-5}m)

Distribution of eccentric mass	q_1	q_2	q_3	q_1'	q_2'	q_3'
Same side	1.8	2.2	1.2	26.9	24.7	27.0
Asymmetric opposite side	2.7	2.7	1.6	26.6	29.3	32.3
Symmetric opposite side	2.7	2.8	1.3	31.6	33.9	31.6

Table 3 Steady-state phase of ball at supercritical speed

(unit: degree)

Distribution of eccentric mass	φ_{11w}	φ_{12w}	φ_{21w}	φ_{22w}	φ_{31w}	φ_{32w}
Same side	-82.1	161.1	-75.3	166.3	-77.4	159.8
Asymmetric opposite side	-83.6	157.0	166.6	-73.0	103.2	-20.3
Symmetric opposite side	155.3	-82.0	-18.2	102.4	164.1	-78.6

The simulation results of the subcritical speed of rotation are shown in fig. 6, 7, 8, while the steady-state resultant amplitude at subcritical speed of rotation is shown in table 4 and the steady-state phase of ball at subcritical speed of rotation is shown in table 5. It shows that the ball is moved automatically to the same side of the eccentric mass; Steady-state resultant amplitude increases significantly when increasing the eccentric mass; The ball is unable to be stable. The resutant amplitude reaches the maximum and has an increasing trend upon 30 s, which shall not exceed the value produced when the ball overlaps the eccentric mass; The resultant amplitude of auto-balancing rotor is multiple times of that of common rotor; Shaft center orbits of auto- balancing rotor and common rotor are hollow circles. Yet auto-balancing rotor has a larger radius and vibration that the common one.

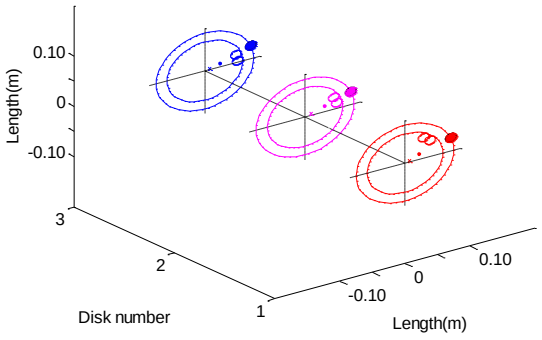

(a) Steady-state location diagram of ball, eccentric mass and centroid

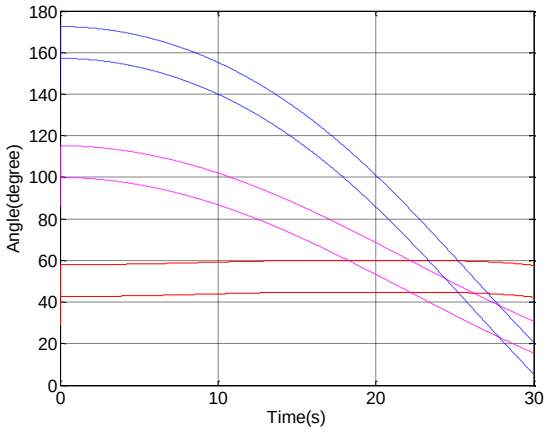

(b) Phase variation process diagram of the ball

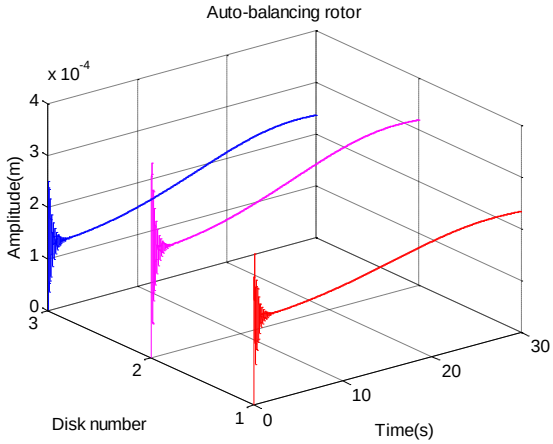

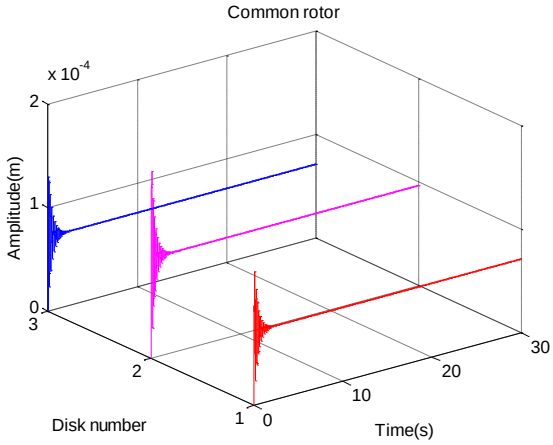

(c) Resultant amplitude diagram of rotor

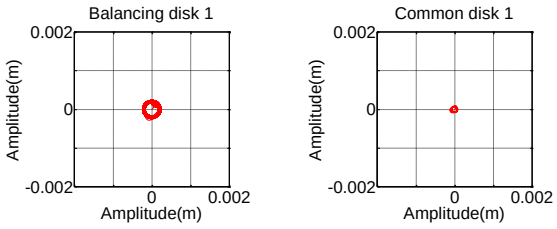

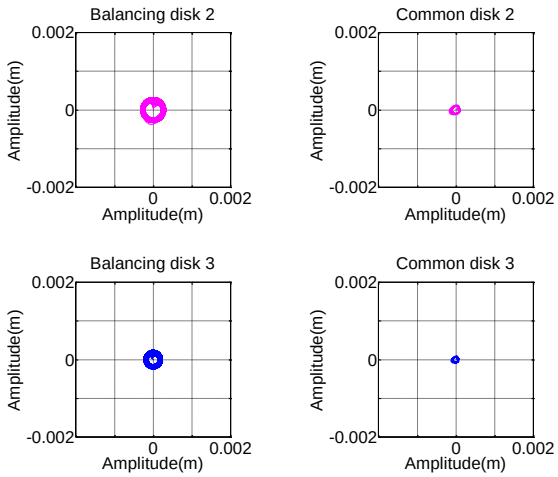

(d) Orbit diagram of the shaft center

Fig. 6 Simulation results of same side distribution whenω =6Hz

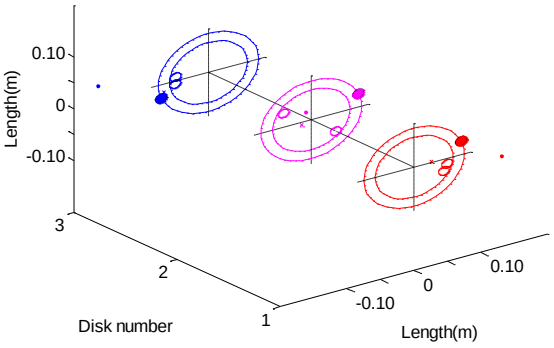

(a) Steady-state location diagram of ball, eccentric mass and centroid

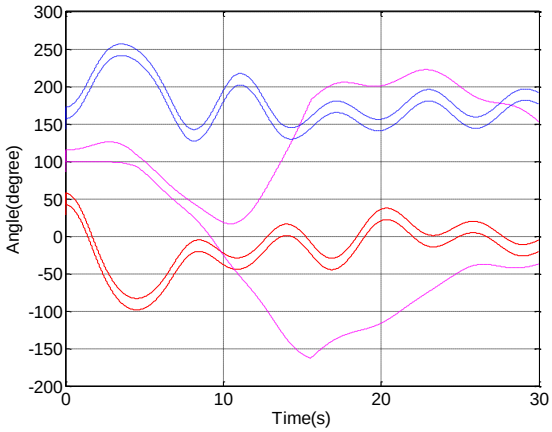

(b) Phase variation process diagram of the ball

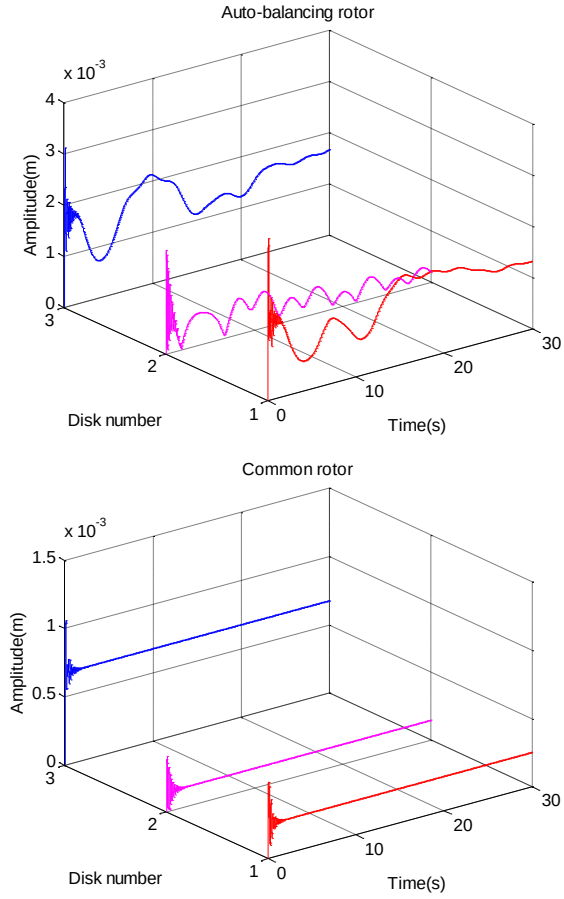

(c) Resultant amplitude diagram of rotor

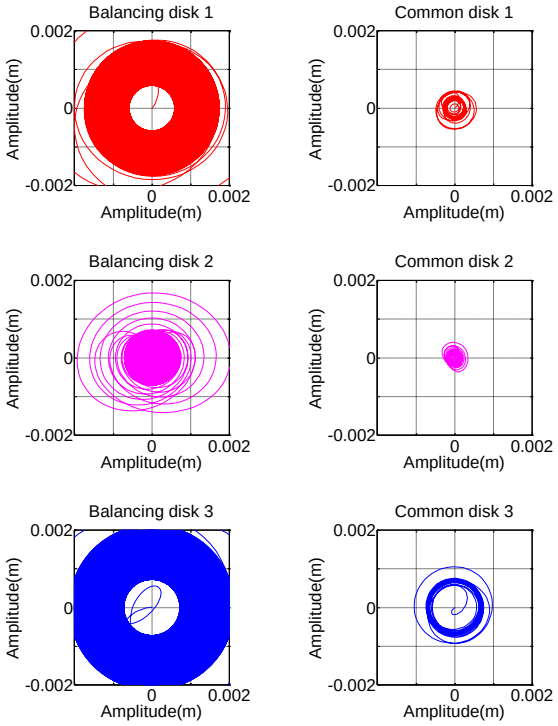

(d) Orbit diagram of the shaft center

Fig. 7 Simulation results of asymmetric opposite side distribution when

ω =20Hz

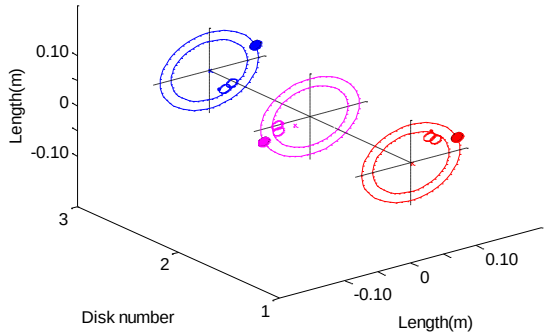

(a) Steady-state location diagram of ball, eccentric mass and centroid

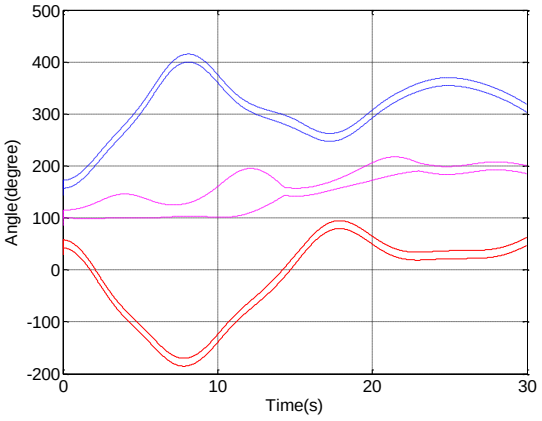

(b) Phase variation process diagram of the ball

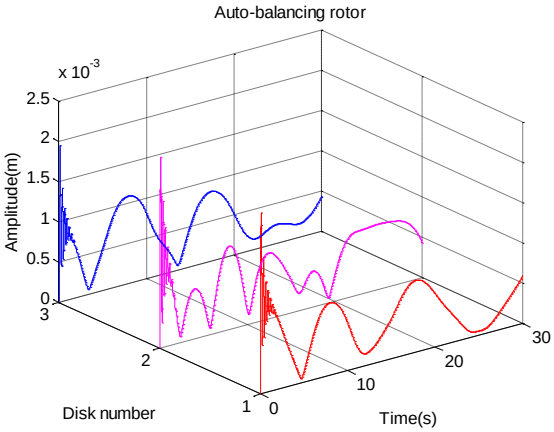

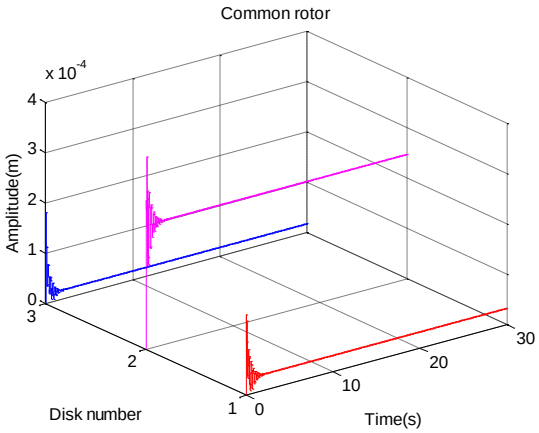

(c) Resultant amplitude diagram of rotor

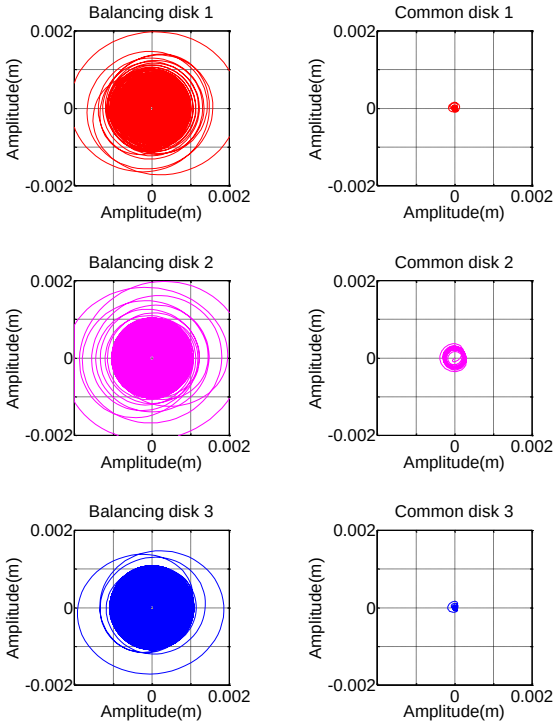

(d) Orbit diagram of the shaft center

Fig. 8 Simulation results of the symmetric opposite side distribution whenω =30Hz

Table 4 Steady-state resultant amplitude at subcritical speed

(unit: 10^{-5}m)

Distribution of eccentric mass	q_1	q_2	q_3	q_1'	q_2'	q_3'
Same side	20	30	20	7	10	7
Asymmetric opposite side	130	20	170	30	10	70
Symmetric opposite side	60	40	40	4	24	3

Table 5 Steady-state phase of ball at subcritical speed

(unit: degree)

Distribution of eccentric mass	φ_{11}	φ_{12}	φ_{21}	φ_{22}	φ_{31}	φ_{32}
Same side	57.7	42.4	30.8	15.5	20.8	5.6
Asymmetric opposite side	-5.1	-20.4	153.1	-37.2	192.0	176.7
Symmetric opposite side	62.2	47.0	200.7	185.4	318.6	303.3

4. Conclusions

The ball was moved automatically to the opposite side of eccentric mass with balancing eccentric mass automatically and reducing vibration when the tri-disk auto-balancing rotor reached above third order critical rotation speed; The ball was moved automatically to the same side of eccentric mass, enlarging eccentric mass and increasing vibration when below first order critical rotation speed; Regarding distributions on the same side, vibration was reduced when they are between first order and second order critical rotation speeds; Regarding distributions on the same side and on the asymmetric opposite side, vibration was reduced, when they are between second order and third order critical rotation speeds; Vibration was increased in other situations.

Notations

m_{pi}= Eccentric mass of the disk i
e_i= Eccentric distance of the disk i
M_{pi}= Quality of the disk i
M_i = Equivalent quality of the disk i
X_i= Displacement of the disk i in the X direction
Y_i= Displacement of the disk i in the Y direction
k_i= Stiffness of the disk i in the X or Y direction
c_i= Damping of the disk i in the X or Y direction
m_{qi}= Quality of ball in the disk i
r_i= Radius of ball in the disk i
R_i= Orbital radius of ball in the disk i
I_i = Rotary inertia of ball in the disk i
β_{i0}= Rolling friction coefficient of ball in the disk i
β_{i1}=Viscous damping coefficient of ball in the disk i
α_i= Eccentric mass phase in the disk i
ϕ_{ij}= Phase of the ball j in the disk i
ϕ_{ij0}= Initial phase of the ball j in the disk i
ϕ_{ijw}= Stable phase of the ball j in the disk i
q_i= Stable amplitude of auto-balancing rotor disk i
q_i'= Stable amplitude of common rotor disk i
ω = Angular velocity of the rotor

Conflict of interest

The authors have confirmed that this article content has no conflict of interest.

Acknowledgment

This research was supported by National Program on Key Basic Research Project of China (2013CB035401); National Natural Science Foundation of China (51274252); National Natural Science Foundation of China (51074180).The authors would like to thank High Performance Computing Center of Central South University for their support in preparing this article.

References

[1]Kim Jong-Soo，Lee Soo- Hun. The Stability of Active Balancing Control Using Influence Coefficients for a Variable Rotor System[J]. The International Journal of Advanced Manufacturing Technology，2003，22(7- 8)：562~567

[2]Bövik, P., Högfors, C.. Autobalancing of Rotors[J]. Journal of Sound and Vibration, 1986, 111(3): 429~440

[3]Wettergren H L. Using guided balls to auto-balance rotors[J]. Journal of Engineering for Gas Turbines and Power, 2002, 124(4): 971~975

[4]Huang W Y, Chao C P, Kang J R, et al. The application of ball-type balancers for radial vibration reduction of high-speed optic disk drives[J]. Journal of Sound and Vibration, 2002, 250(3): 415~430

[5]Lutz Sperling,Falk Merten,Henner Duckstein. Self-synchronization and Automatic Balancing in Rotor Dynamics[J]. International Journal of Rotating Machinery，2000，6(4)：275~285

[6]Van De WouW, N., Van Den Heuvel, M. N., Nijmeijer, H., and Van Rooij, J. A. Performance of an Automatic Ball Balancer with Dry Friction[J] . International Journal of Bifurcation and Chaos, 2005, (15): 65~82

[7]Green, K. M. I., Friswell, A. R., Champneys, and N. A. J. Lieven . The Stability of Automatic Ball Balancers[J]. Proceedings of ISCORMA, 2005, (3): 457~465

[8]K.Green，A.R.Champneys，N.J.Lieven. Bifurcation analysis of an automatic dynamic balancing mechanism for eccentric rotors[J]. Journal of Sound and Vibration, 2006, (291): 861~881

[9]K. Green,A.R. Chanpneys,M.I. Friswell. Analysis of the transient response of an automatic dynamic balancer for eccentric rotors[J]. International Journal of Mechanical Sciences, 2006, (48): 274~293

[10]D.J. Rodrigues,A.R. Champneys,M.I. Friswell,R.E. Wilson. Experimental investigation of a single-plane automatic balancing mechanism for a rigid rotor[J]. Journal of Sound and Vibration, 2011, (330): 385~403

[11]J. Ehyaei,Majid M. Moghaddam. Dynamic response and stability analysis of an unbalanced flexible rotating shaft equipped with n automatic ball-ball-balancers[J]. Journal of Sound and Vibration, 2009, (321): 554~571

[12]Yukio Ishida. Recent development of the passive vibration control method[J]. Mechanical Systems and Signal Processing, 2012, (29): 2~18

Associate Prof. YANG Yi-jiao , Address correspondence to YANG Yi-jiao at the State Key Laboratory of High Performance Complex Manufacturing, Central South University, Changsha, Hunan 410083, China;

Prof. TAN Qing , Address correspondence to TAN Qing at the State Key Laboratory of High Performance Complex Manufacturing, Central South University, Changsha, Hunan 410083, China;

YI Nian-en (Corresponding Author) is working on the rock breaking mechanics of TBM (tunnel boring machine) cutters and design problems. To improve the cutting performance and prolong cutter life. Address correspondence to corresponding author at the School of Mechanical and Electrical Engineering, Central South University, Changsha, Hunan 410083, China;